Composite Structures 99 (2013) 112–122

Contents lists available at SciVerse ScienceDirect

Composite Structures

journal homepage: www.elsevier.com/locate/compstruct

Punching shear strengthening of two-way flat slabs using CFRP rods

M. Hasan Meisami [a,*], Davood Mostofinejad [a], Hikaru Nakamura [b]

[a] Department of Civil Engineering, Isfahan University of Technology (IUT), Isfahan, Iran
[b] Department of Civil Engineering, Nagoya University, Nagoya, Japan

ARTICLE INFO

Article history:
Available online 20 December 2012

Keywords:
A. Carbon fiber
B. Debonding
C. Analytical modeling
Slab strengthening

ABSTRACT

The results of an experimental program on two-way reinforced concrete (RC) flat slabs under punching shear due to central loading are presented in this paper. All the six RC slabs were designed according to ACI 318-08 code provisions. Two slabs served as control without any modification while the other four were strengthened in different ways: one with M16 screws and nuts, and three with CFRP rods. For strengthening in each case, 8 and 24 strengtheners were used. A method is proposed for predicting maximum loading capacity of slabs strengthened with CFRP rods and with epoxy resin in drilled holes. The results of the experiments showed that the selected strengthening method was not only able to improve the maximum loading and deformation capacity of the slabs but also avoided brittle failures likely to occur under vertical point loadings.

1. Introduction

Despite their wide applications in buildings and bridges in the past, reinforced concrete (RC) flat slabs have recently become a source of concern for their vulnerability to damage or failure in many old structures due to changes both in their usage and loading and in the relevant updated design codes. As a remedy to this situation, much attention in recent years has been focused on strengthening RC flat slabs. Attempts by many investigators to increase the shear capacity of existing slabs include, but are not restricted to, adding steel bars, steel rods, and shear bolts; steel jacketing; increasing column size; and applying FRP sheets or stirrups.

Hassanzadeh and Sundqvist [1] showed that insertion of steel bars into drilled holes around the slab–column connection would increase the punching failure load by up to 55% compared to the un-strengthened control. They used column heads (a steel collar bonded to the slab and the column) in two experiments for doubling and tripling column diameter and observed increases in the punching shear capacity equal to 60% and 100%, respectively. Polak [2] showed that existing connections strengthened with shear bolts had almost the same strength as new connections with shear studs, both exhibiting very similar load–deflection characteristics. Polak [2] found that the presence of shear bolts increased ultimate loading and deformation capacities of the connection, while the deformation capacity of the connection also increased with the number of peripheral rows of shear bolts, forming a punching cone outside the shear reinforced zone.

Martinez-Cruzado et al. [3] strengthened post-tensioned slab–column connections to improve their seismic behavior by installing two steel plates on the top and bottom sides of the slab. The specimens strengthened with steel jackets exhibited stiffness, strength, and deformability properties superior to those of the original connection but similar to those of the connection repaired with column capitals. To study the use of a tightly-knit array of externally installed CFRP stirrups for both monotonic concentric and eccentric load tests, Binici [4] experimented concrete slabs strengthened with a high amount of flexural reinforcement (ρ = 1.76%). It was shown in the Binici's study that using externally installed CFRP stirrups with sufficient anchorage for the vertical legs to improve the two-way shear strength and residual capacity of slab–column connections would increase the punching shear, deformation, and post-punching capacities of the connection.

Erki and Heffernan [5] used FRP sheets on the tension surface of the slab and observed that both flexural stiffness and punching shear capacity of the slabs improved while the flexural cracking was delayed. Harajli and Soudki [6] found that CFRP sheets on the tension face of the connection improved flexural and shear capacities by about 17–45%; they, however, suspected that the increase in flexural strength by CFRP sheets might change failure from a flexural to a punching shear mode. The CFRP sheets bonded to the tension side of the slabs did not change the location of punching shear failure surface significantly. El-Salakawy et al. [7] combined FRP sheets and steel bolts to observe increased connection ductility and ultimate strength along with a change in the failure pattern from the punching to the flexural mode.

* Corresponding author. Address: Civil Engineering Department, Isfahan University of Technology (IUT), Post Box: 8415684111, Isfahan, Iran. Tel.: +98 311 391 2701; fax: +98 311 391 2700.

E-mail addresses: meisami@cv.iut.ac.ir, mhm7050@gmail.com (M.H. Meisami), dmostofi@cc.iut.ac.ir (D. Mostofinejad), hikaru@nagoya-u.jp (H. Nakamura).

0263-8223/$ - see front matter © 2012 Elsevier Ltd. All rights reserved.
http://dx.doi.org/10.1016/j.compstruct.2012.11.028

Mosallam and Mosalam [8] studied the ultimate capacity of two-way slabs repaired with CFRP strips. Before the repair, the slabs were loaded up to 85% of their ultimate capacity. The ultimate capacity of the repaired slabs was approximately 198% higher than that of the control slab and the failure was preceded by relatively large deformations. Mostafa [9] studied the effectiveness of comb-shape NEFMAC anchors, which was drew out from NEFMAC grid. The comb teeth were inserted into drilled-holes and the comb spine was bonded to the FRP sheets. The anchors were effective in delaying delamination. Stark [10] studied the application of CFRP stirrups that externally installed on the slabs for seismic applications. The study showed that the externally installed CFRP stirrups provide an alternative method for improvement of existing flat-plate slab–column connections for seismic performance.

Since FRP composites have been practically found to be very effective and easy-to-use materials for strengthening purposes in the past decade, it seems that use of FRP rods anchored in drilled holes with epoxy resins may also provide an easy and suitable procedure for punching shear strengthening of RC two-way slabs. Higher tensile strength of FRP rods compared to steel bars may decrease the number of FRP bolts required for punching shear strengthening compared to number of required steel bars, leading to less labor works and expenses. To examine the applicability of FRP rods for shear strengthening, the punching shear behavior of concrete slabs strengthened with CFRP rods and epoxy resin in drilled holes is investigated in the current study. Furthermore, the failure mechanism of punching shear after strengthening is studied and an expression is developed for predicting the punching shear capacity of two-way flat slabs strengthened with CFRP rods.

2. Experimental program

2.1. Test specimens

Six concrete slabs of identical lengths and widths but different depths were constructed and strengthened with identical steel-reinforcement ratios. The preliminary design of the slabs was accomplished using the appropriate software to choose a proper reinforcement ratio according to real loads in common structures. Spans of the structure analyzed were 4.0 m by 4.0 m bays in two directions with 5 kN/m^2 live and 4 kN/m^2 dead loads in addition to the slab self weight due to a depth of 105 mm. The cast slabs were 1200 mm long $\times$ 1200 mm wide with two different depths of 85 and 105 mm. Fig. 1 shows the slab layout and reinforcement arrangement in one series of the slabs. The top steel bars were chosen as $\varnothing$6 while the bottom ones varied due to differences in reinforcement ratios used. Table 1 shows the details of reinforcement and arrangement of the test specimens.

The specimens comprised of two control slabs used for comparison and four strengthened slabs; one strengthened with screws and nuts, and three post-casts strengthened with FRP rods installed by an epoxy adhesive. Specimen details are summarized in Table 2. In order to determine the lower and upper limits of strengthening and punching shear capacity and in order to properly install screw bolts and FRP rods in the slabs around the 150 $\times$ 150 mm loading plate in the center of the slabs, two arrangements of type A and B with 8 and 24 strengthening screw bolts and FRP rods, respectively, were used as shown in Fig. 2.

2.2. Material properties

The steel reinforcing bars used consisted of $\varnothing$6 and $\varnothing$16 with yield strength of 420 MPa, and $\varnothing$10 with yield strength of 345 MPa. The Leadline FRP rods were 12.5 mm in diameter produced by Mitsubishi Chemical Corporation in Japan using pultrusion method. Leadline bars are composed of pitch-based carbon fibers and epoxy resin; where fibers' volume fraction is 65%. The rods had 1400 MPa ultimate strength, 0.015 ultimate strain, and 120,000 MPa Young's modulus according to the manufacturer's (NCK Co.) certificate; also based on ancillary tests carried out in laboratory. The M20x150 screw and nut had two end bearings 16 mm in diameter and with a yielding stress of 320 MPa and an ultimate strength of 400 MPa. Fig. 3 gives a picture of the assembly together with the material properties of the steel and CFRP rods used.

The concrete used had a compressive strength of 35 MPa and a mix proportion as in Table 3. The strengths achieved after 28 days

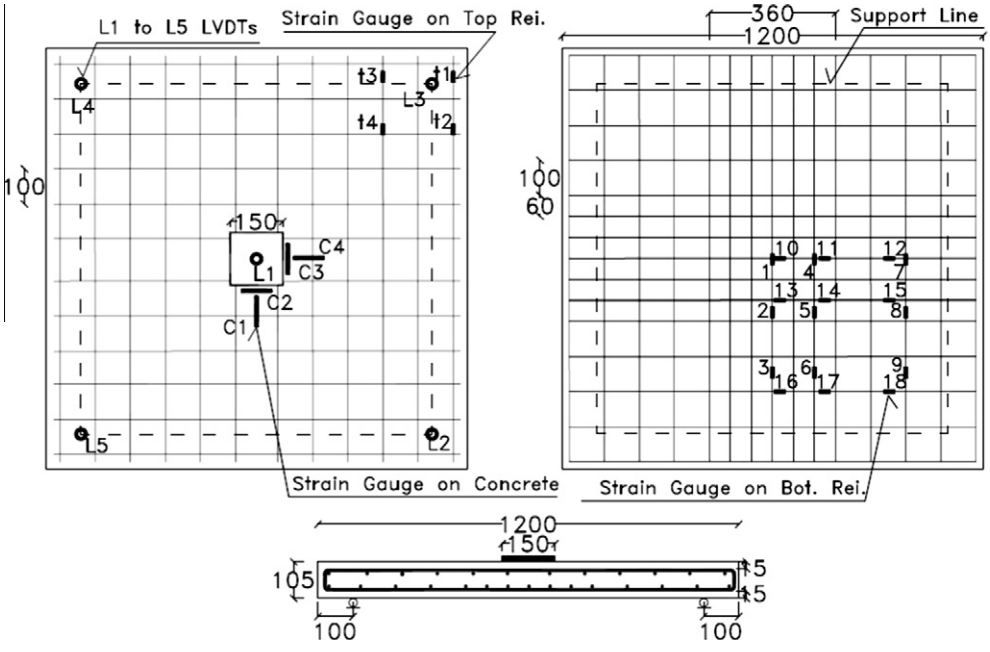

Fig. 1. Slab layout and reinforcement arrangements (L1–L5 refer to LVDTs, and C1–C4, t1–t4 and 1–18 refer to strain gauges on concrete, on top reinforcement and bottom reinforcement, respectively).

Table 1
Details of reinforcement and arrangement of test specimens.

	Height (mm)	Bot. rein.	Top rein.	Gauge no.	LVDTs no.
Arrangement 1	85	15∅10; ρ = 1.10%	12∅6; ρ = 0.38%	12 + 4	5
Arrangement 2	105	11∅16; ρ = 2.20%	11∅6; ρ = 0.35%	10 + 4	5

Table 2
Details of test specimens.

Test no.	Specimen name	Type	Strengthener	Bottom rein.	Top rein.	f'_c (MPa)
1	CS40-2	Control	–	15∅10	12∅6	41.1
2	FR2-8	FRP rod + epoxy, AC[a]	8 FRP, ∅12	15∅10	12∅6	36.6
3	SN2-8	Screw and nut + epoxy, AC[a]	8 Screw, M16	15∅10	12∅6	37.7
4	CS40-3	Control	–	11∅16	11∅6	42.4
5	FR3-8	FRP rod + epoxy, AC	8 FRP, ∅12	11∅16	11∅6	43.5
6	FR3-24	FRP rod + epoxy, AC	24 FRP, ∅12	11∅16	11∅6	43.5

[a] AC means after casting installation of strengthener.

are reported in Table 2. FRP rods were installed in slabs after casting by inserting rods in prepared slots in fresh concrete. A two-component epoxy adhesive resin was also used. The shear and tensile strengths of the epoxy resin used were 10 MPa each after curing for 6 h at 20 °C or for 1 day at 5 °C and at ambient humidity as instructed by the manufacturer. The resin epoxy used for adhering the FRP bolts into the drilled holes were cured at least for 1 week at laboratorial ambient temperature (about 30 °C) and relative humidity equal to 80% before performing the tests.

2.3. Test procedure

All the specimens were tested under monotonic central load until failure. In some cases, unloading was done two or three times before failure. Load was applied on rigid 150 × 150 × 30 mm steel plates using a hydraulic jack. Load application was accomplished manually under displacement control so that load displacement rate could be kept near the shear punch of the slab and within the hydraulic jack capacity (Fig. 4).

Displacements were measured by 5 LVDTs (linear variable displacement transducers) with a gauge length of 25 mm. One transducer was placed centrally on the bottom side of the slabs to measure maximum displacement while 4 others were placed on the top corners of the slabs to measure uplifts at corner points as these points were free of movement. The average displacement value obtained from the central transducer was used as the relative displacement for establishing the load–displacement relation. Fig. 1 shows LVDTs L1–L5.

Strain gauges were installed on steel reinforcement in two directions, on the concrete surface of the slab top and on the FRP rods. The number of strain gauges for each slab arrangement is reported in Table 1 and one gauge is shown in Fig. 1, in which numbers 1–18 refer to bottom strain gauges, t1–t4 designate top strain gauges, and C1–C4 designate the strain gauges mounted on the top surface of the slabs for measuring the strain in concrete. The data reading procedure was continued until failure occurred in the slabs during shear punch or after flexural behavior was observed in slabs. The relationship between the data obtained for

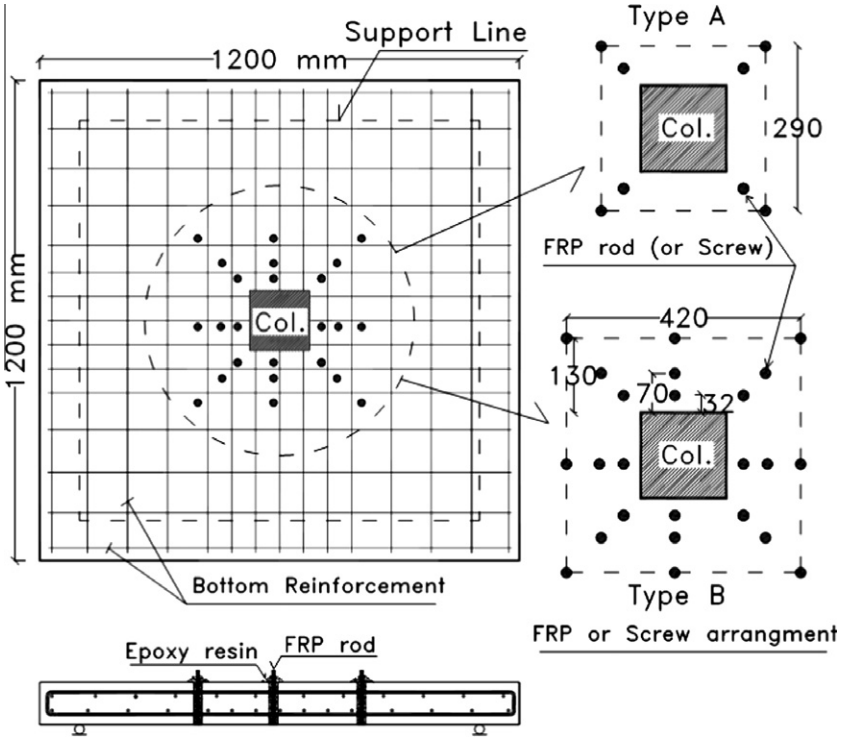

Fig. 2. FRP rods and screw arrangements on slab around column (8 and 24 strengthener positions around column for type A and B, respectively).

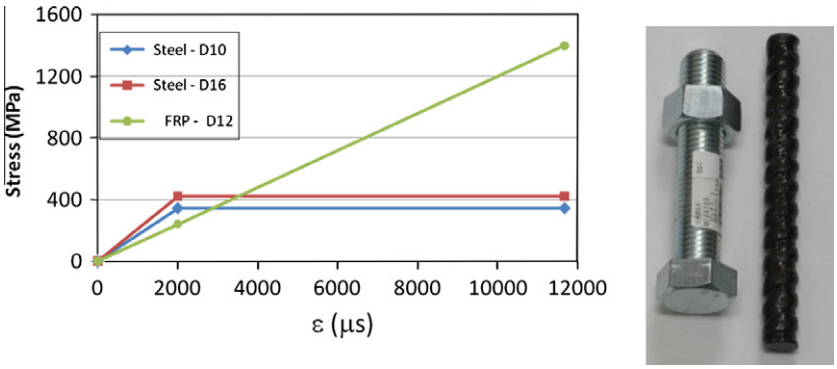

Fig. 3. Material properties reported by the manufacturers.

Table 3
Concrete mix proportion and strength.

f'_c (MPa)	W/C	s/a	d_{max} (mm)	W (kg/m^3)	C (kg/m^3)	S (kg/m^3)	G (kg/m^3)
35	0.6	45	20	175	292	775	962

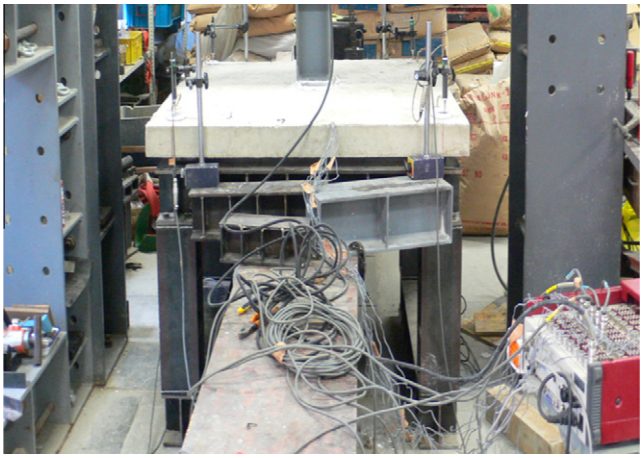

Fig. 4. Test setup for loading of slabs.

reinforcement strain distribution and those of load–displacement will be discussed in the following section.

3. Experimental results and discussion

3.1. Load–displacement response

The load–displacement relationships for the control slabs CS40-2 and CS40-3 are shown in Fig. 5. As can be seen in Table 1, the slabs are different with respect to their reinforcement types and ratios. The values for reinforcement ratio and yielding strength in the case of CS40-2 are 1.1% and 345 MPa, respectively, while those for CS40-3 are 2.2% and 420 MPa, respectively. Fig. 5 indicates that doubling the reinforcement ratio increased the punching shear capacity by around 9% from 224.1 to 241.7 kN accompanied by a slight increase in concrete compression strength from 41.1 to 42.4 MPa.

Flexural capacity of the slabs per unit width is given by Eq. (1). Flexural punching and pure punching shear, respectively, may be calculated using Eqs. (2) and (3) proposed by Moe [11].

$$m = \rho f_y d^2 \left(1 - 0.59\rho\frac{f_y}{f'_c}\right) \quad (1)$$

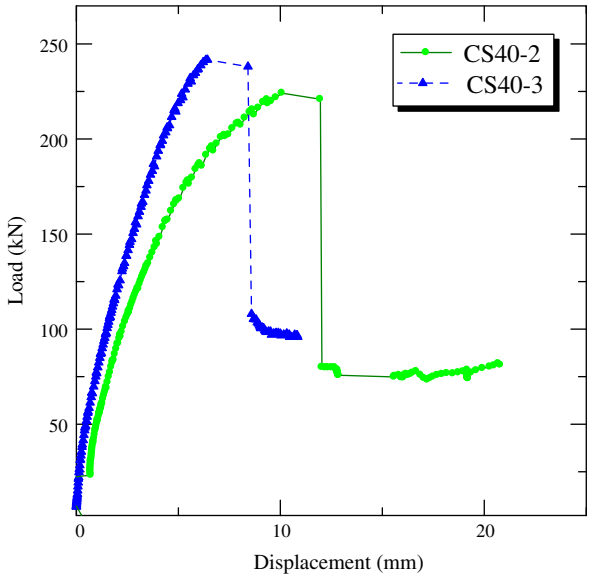

Fig. 5. Load–displacement relationship of control slabs CS40-2 and CS40-3.

$$V_{flex} = 8m\left(\frac{1}{1-\frac{c}{a}} - 3 + 2\sqrt{2}\right) \quad (2)$$

$$V_u = \frac{1.25\left(1 - 0.075\frac{c}{a}\right)\sqrt{f'_c}}{1 + \frac{0.44u_0 d\sqrt{f'_c}}{V_{flex}}}u_0 d \quad (3)$$

where ρ is the reinforcement ratio; f_y is steel strength in MPa; f'_c is concrete compressive strength in MPa; d and a are the effective depth and width of the slab, respectively; c and u_0 are column or loading plate width and perimeter, respectively; m is the flexural capacity per unit length; V_{flex} is the shear strength corresponding to the flexural punching; and V_u is the pure punching shear of the slabs. Table 4 reports the values of these parameters calculated using the presented equations for all the test slabs. In this table, b_0 and b'_0 designate the perimeter of the punching shear area around the plate load before and after strengthening for the two types A and B in Fig. 2.

Table 4
Calculated loads for test specimens.

Test no.	Specimen name	d (mm)	b_0 (mm)	b_0' (mm)	c (mm)	a (mm)	u_0 (mm)	f_y (MPa)	ρ	V_{flex} (kN)	V_u (kN)	P_{Test} (kN)	Failure mode
1	CS40-2	80.5	921.9	921.9	150	1000	600	345	0.01	202.6	199	224.1	Shear
2	FR2-8	80.5	921.9	1161	150	1000	600	345	0.01	201.1	192	248	Shear
3	SN2-8	80.5	921.9	1161	150	1000	600	345	0.01	201.5	194	257.9	Flexural
4	CS40-3	74.1	896.4	896.4	150	1000	600	420	0.02	368.6	228	240.4	Shear
5	FR3-8	74.1	896.4	1160	150	1000	600	420	0.02	370	230	286.2	Shear
6	FR3-24	74.1	896.4	1680	150	1000	600	420	0.02	383.1	234	412	Flexural

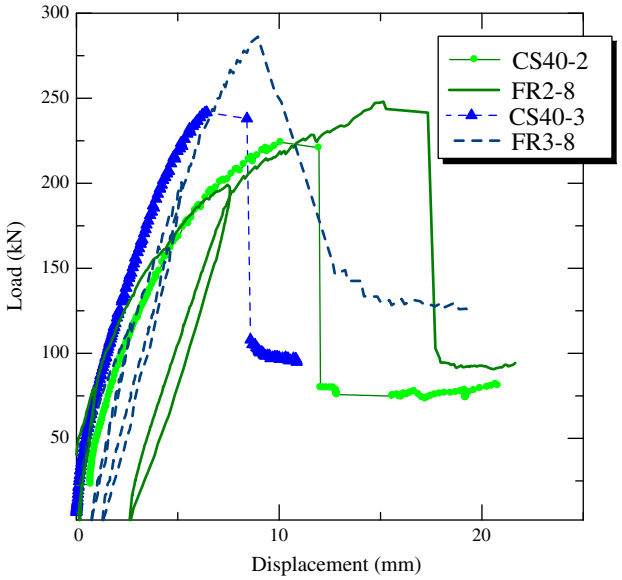

Fig. 6. Load–displacement relationship for slabs FR2-8 and FR3-8 and their corresponding controls.

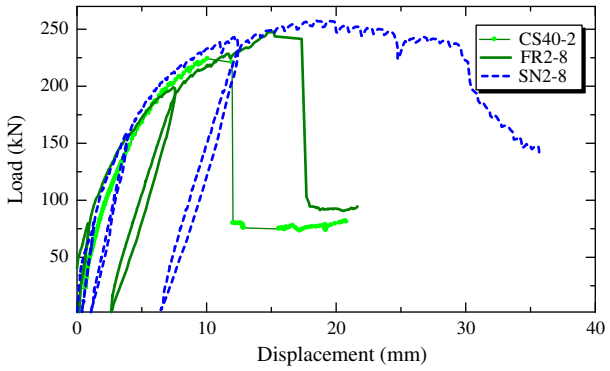

Fig. 7. Load-displacement relationship for slabs SN2-8 and FR3-8.

Fig. 8. Screw and nut verses FRP rods setup in slabs.

The load–displacement relationships for strengthened slabs using 8 FRP rods and the corresponding controls are presented in Fig. 6. Both FR2-8 and FR3-8 were strengthened using eight CFRP rods 12.5 mm in diameter. The differences between these two slabs arise from the change in their reinforcement ratios and the resulting values of concrete compression strength, which were measured to be 36.6 and 43.5 MPa for FR2-8 and FR3-8, respectively. Comparison of the control, CS40-2, with the strengthened FR2-8 slab reveals a slight increase in the shear capacity of the latter as compared to the higher compression strength of the former. This indicates that FRP rods in this case increased shear capacity by 11%. Comparison of the control slab, CS40-3, with the strengthened FR3-8 slab indicates an increase of 19% in shear capacity.

Due to the large variations in the values of concrete compression strength obtained from the cylinder test, a more accurate comparison was made possible when the results were normalized by multiplying loads by $\sqrt{f'_{c,control}/f'_{c,test}}$. The normalized values for all the specimens are reported in Table 5, in which more experimental details are also provided. In this table, P_y designates the load for which the first longitudinal reinforcement yields and δ_y is the corresponding displacement; P_u is the maximum load obtained with δ_u being its corresponding displacement; and the ductility factor is the ratio of δ_u to δ_y. Once the values were normalized, an increase of 17% was obtained for the punching shear ratio for FR2-8. Punching shear exhibited an increase of 19% in its as-obtained value and an increase of 16.9% in its normalized value in the two FR3-8 strengthened slab and CS40-3. The decreasing ratio in this case could be attributed to the lower concrete strength of FR3-8 compared to that of CS40-3. A similar

Table 5
Test details: load, displacement, and normalized load values.

Test no.	Specimen name	Test, f'_c (MPa)	P_y (kN)	P_u (kN)	$P_{y,n}$ (kN)	$P_{u,n}$ (kN)	δ_y (mm)	δ_u (mm)	Ductility
			Real forces		Normalized forces				
1	CS40-2	41.1	146.1	224.1	146.1	224.1	5.3		1.89
2	FR2-8	36.6	158.1	248	167.5	262.9	5.4	15.1	2.80
3	SN2-8	37.7	204.6	257.9	213.6	269.3	6.7	18.4	2.75
4	CS40-3	42.4	225.9	241.7	225.9	241.7	6.4	6.4	1.00
5	FR3-8	43.5	247.8	286.3	244.7	282.6	6.8	8.9	1.31
6	FR3-24	44.1	303	412	297.1	404	7.1	29.3	4.13

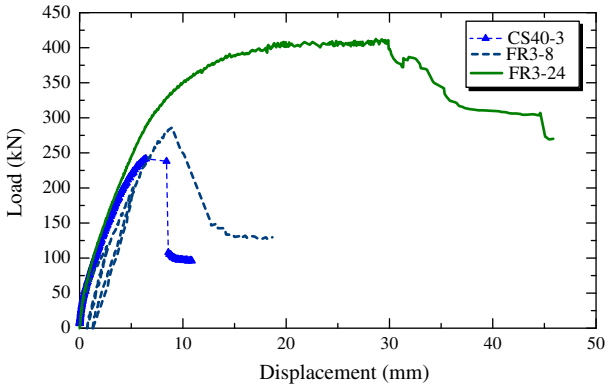

Fig. 9. Load–displacement relationship for slabs FR3-24, FR3-8 and CS40-3.

(a) CS40-2, shear cone;

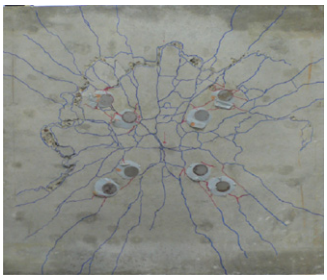

(d) FR2-8, shear cone;

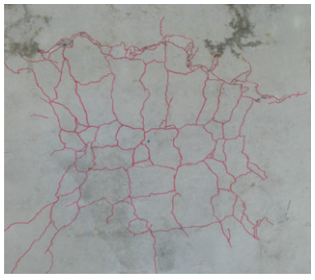

(b) CS40-3, shear cone;

(e) FR3-8, shear cone;

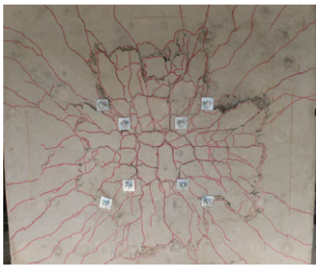

(c) SN2-8, shear cone & flexural expansion

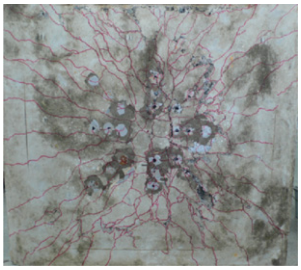

(f) FR3-24 shear cone and flexural expansion

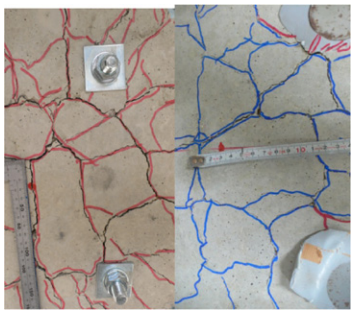

(g) Near view of cracks

Fig. 10. Tension surface crack patterns of all the specimens after failure.

increase was observed in the case of both FR2-8 and FR3-8 compared to their corresponding control slabs. On the other hand, comparison of FR2-8 and FR3-8 revealed an increase of 7.6% in the normalized values that must be due to the reinforcement ratio and concrete strength. This observation is in agreement with the results obtained for the control slabs CS40-2 and CS40-3.

Fig. 7 shows the load–displacement relationship for the slab SN2-8, which was strengthened using eight M20 screws and nuts with end bearing plates at both ends, and the corresponding FR2-8, which was strengthened in a similar fashion using 8 FRP rods (see Fig. 3). The differences observed involve two different aspects of the slabs. The first involves the fact that the most distinctive difference observed between the two lies in the patterns of their flexural and brittle punching shear behavior. Two causes may be claimed for this difference in behavior. The first involves differences between the end bearings and bond effects around FRP rods and the screws-and-nuts. The second stems from differences in material properties of screws and nuts used in SN2-8 compared with those of FRP rods used in FR2-8 slabs; as seen in Fig. 3, while steel exhibits a ductile behavior after yielding, FRP undergoes a sudden rupture. Compared to the control slab CS40-2, SN2-8 exhibits increases by 15% and 20.1% in shear capacity for as-obtained and normalized values, respectively; i.e., 4% and 3% higher than those obtained for FR2-8 under similar conditions. These results indicate that strengthening with FRP rods yields almost the same results as those obtained when screws are used despite the fact that the cross area of FRP rods is less than half that of the screws (118 m^2 in the case of FRP rods and 265 m^2 in the case of M20 screws). Since maximum loading is limited to the flexural load capacity in SN2-8, its maximum capacity is exploited because the slab uses two mechanisms to transfer load to the screws, namely end bearing and epoxy bonds. In FR2-8, however, only the bond through epoxy is available for transferring the load to FRP. Thus, a fully flexural behavior is not observed but the shear capacity increases and a slightly flexural behavior is seen.

The second aspect involves the attachment mechanisms used. Screws were placed in the slab SN2-8 using two types of attachment simultaneously; namely, nuts and bearing plates for both ends fastened tightly in proportion to their maximum capacity while epoxy was also used to fill the spaces between the concrete and the screws (Fig. 8). In the cases of FR2-8 and FR3-8, however, only epoxy was used for bonding FRP rods into the slabs with no end bearing area (Fig. 8). The fact that epoxy can be used to bond FRP rods onto the concrete despite the absence of end bearing areas means that plain FRP rods with an epoxy resin can be used for strengthening the punching shear of slabs.

Fig. 9 illustrates the last test load–displacement relationship for FR3-24 strengthened with 24 FRP rods as compared to its corresponding control slab, CS40-3, as well as FR3-8 strengthened with 8 rods. Due to differences in concrete compression strength, the normalized loads presented in Table 5 are used for comparisons. The maximum loads for CS40-3, FR3-8, and FR3-24 were 241.7, 282.6, and 404 kN, respectively. This indicates a significant increase of 67.2% in FR3-24 compared to the corresponding control, i.e. CS40-3, and an increase of 43% compared to FR3-8. Evidently, a change is observed in the slab behavior. In FR3-8 with 8 FRP rods, the slab still showed a shearing behavior and failed after a brittle drop under its maximum load as did the control. In FR3-24 with 24 FRP rods, a change from shear to flexural behavior occurred. Since in both cases the load is transferred only through the epoxy from concrete to FRP rods inside the slab, it is essential for the bond effect around FRP rods to have sufficient capacity for transferring loads to the high-strength FRP rods. It should also be mentioned that although FRP is brittle compared to steel, it would be possible to achieve flexural behavior in the FRP-strengthened slab so that it exhibited a ductile behavior. The importance of the re-

sults obtained in this case will become more evident if it is noticed that the contact between concrete and FRP rods was only established through the epoxy resin to a depth of 105 mm inside the slab while no end bearing equipment was used. The conclusion to be drawn is that epoxy resin is capable of producing a sufficient bond effect around FRP rods. Using FRP rods with epoxy resin can, therefore, be claimed to be a reasonably adequate method of strengthening slabs despite the small length of contact it creates between the concrete and the FRP rods. An important consideration in the use of epoxy resin is that it is time-dependent, requiring due consideration to its shrinkage and the associated effects. Therefore, epoxy resin must be cured through time in order for it to reach its acceptable strengths. In the present study, a curing time of at least 1 week was allowed for each slab after epoxy application.

3.2. Crack propagation and failure mode

Fig. 10 presents tension surface crack patterns after failure. In all the specimens, crack propagation due to flexural rebar typically started during the initial stages of loading in two weak and strong directions perpendicular to each other. By increasing the load, diagonal cracks started from the center of the slab under point loads and propagated toward the edges, especially toward the corners. Figs. 10 and 11 depict the crack patterns observed in CN40-2 and CN40-3, respectively.

The punching shear areas developed on the tension surfaces of all the strengthened slabs (FR2-8, FR3-8, FR3-24, and SN2-8) can be easily seen. These areas are associated with separation from the surface and crack widths can be measured (Fig. 11). Differences can be recognized in behavior among the slabs; it can be seen that only a shear punch area was produced at the center in slabs exhibiting the shear behavior (i.e., slabs CN40-2, CN40-3, FR2-8, and FR3-8) while in those with the flexural behavior (i.e., SN2-8 and FR3-24), cracked lines extended to the edges and corners after a shear punch area developed.

Fig. 11 shows the punching shear areas developed around the plate on the compression surface (top side) of the slabs CS40-2, CS40-3, SN2-8, and FR3-24. This area entirely developed near plate loads in slabs CS40-2 and CS40-3 because no strengthening mechanism had been deployed inside the slabs. The expanding punching shear area on the compression (top side) surface of SN2-8 and FR3-24 and the propagation of cracks on the sides of the slabs near the corners can also be seen in Fig. 11. It is worth noting that in this case, the shear punch area moved from around the plate to a new place between the screw positions in SN2-8 as a result of strengthening the slabs. This, in turn, caused the shear to increase and to move toward the area outside the FRP rod positions in FR3-24, which led to a significant increase in the shear capacity and to a change from the shear to the flexural behavior.

3.3. Steel and FRP strains

Fig. 12 shows strain distributions in longitudinal steels (as ST-St) during loading for the control slab CS40-3 and the strengthened ones FR3-8 and FR3-24 along with the corresponding

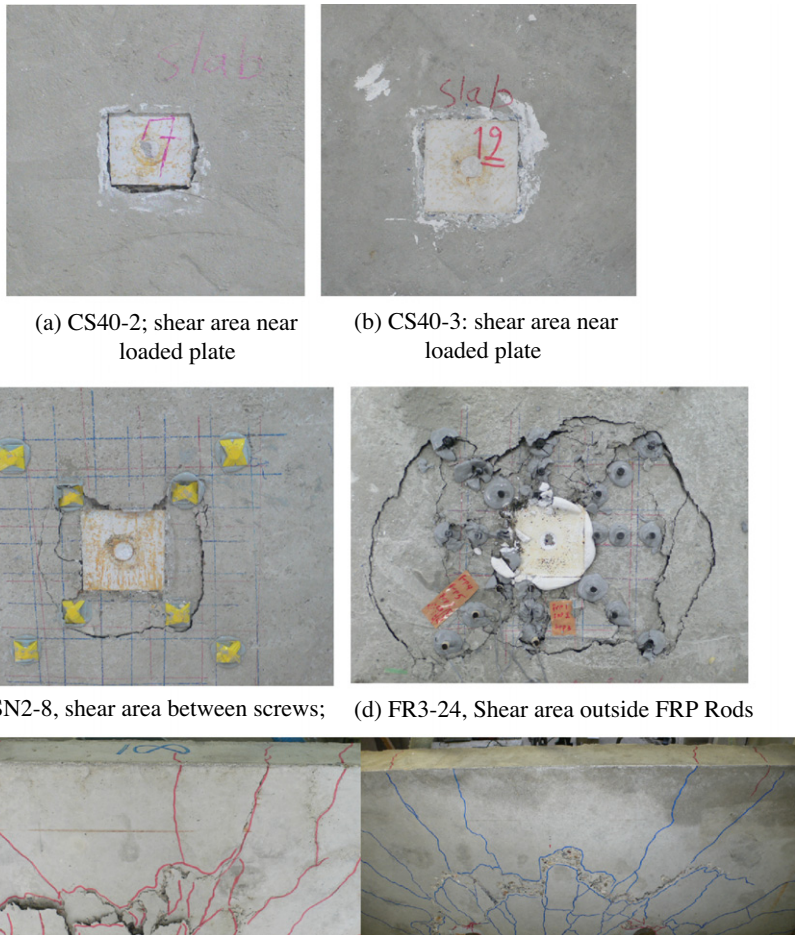

(a) CS40-2; shear area near loaded plate

(b) CS40-3: shear area near loaded plate

(c) SN2-8, shear area between screws;

(d) FR3-24, Shear area outside FRP Rods

(e) propagation of cracks in the sides

Fig. 11. Punching shear area on top of the slabs CS40-2, CS40-3, SN2-8 and FR3-24 and propagation of cracks in the sides.

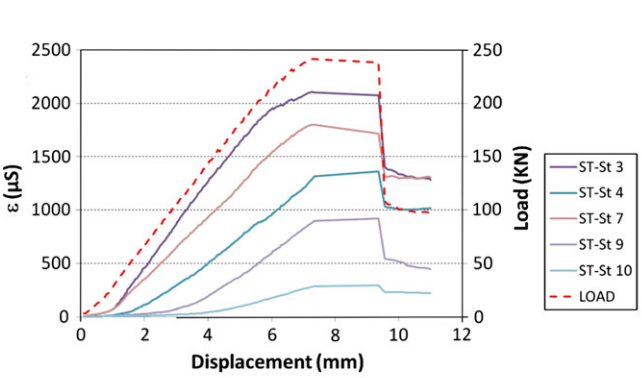

(a) Longitudinal Steel Strain, CS40-3

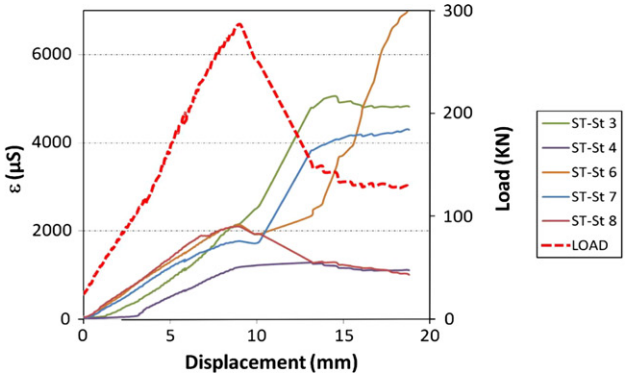

(b) Longitudinal Steel Strain, FR3-8

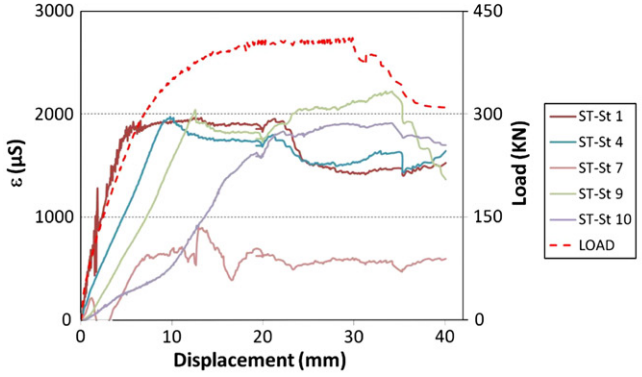

(c) Longitudinal Steel Strain, FR3-24

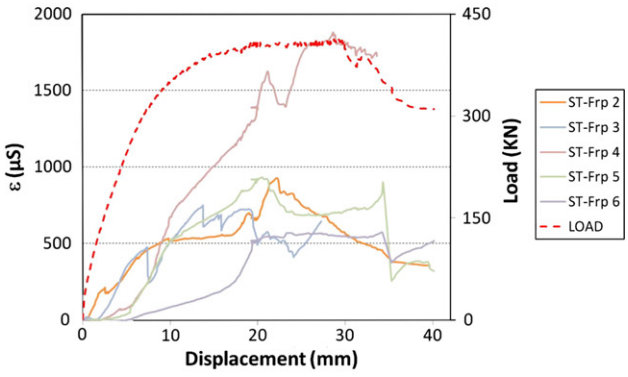

(d) Vertical FRPs Strain, FR3-24

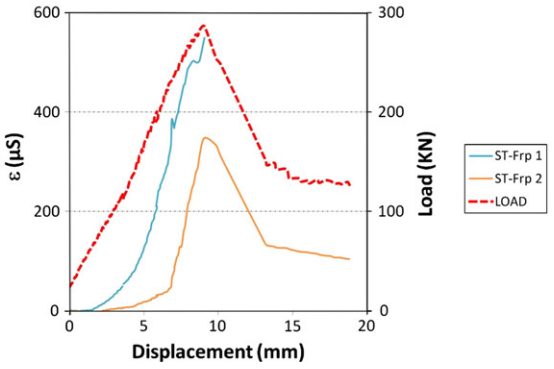

(e) Vertical FRPs Strain, FR3-8

Fig. 12. Strain distribution in longitudinal steels and FRP rods.

load–displacement in each case. In the case of CS40-3 showing a completely shear behavior, the strains observed are far lower than its yielding strain. In the case of FR3-8 with 8 FRP rods, the observed strains were lower than the steel yielding strain before the peak load but it subsequently rose to 0.002. This indicates that strengthening led to an increased loading capacity in the slabs. In FR3-24 with 24 FRP rods, most of the steel strains reached or exceeded 0.002, indicating that FRP rods increased the shear capacity of the slab until a maximum value was reached causing the reinforcements to yield followed by a flexural behavior in the slab. The maximum load in this case was 412 kN before failure.

Fig. 12 also shows the strains in FRP rods (as ST-Frp) in the slabs FR3-8 and FR3-24. The strain increased after reaching a load of about 250 kN corresponding to the maximum load of the control. This is taken to confirm the finding that FRP rods contribute to improved slab behavior by increasing the punching shear capacity and by changing the failure mode.

4. Load prediction for strengthened slabs

It may be inferred from the pattern of cracks shown in Fig. 10 that insertion of FRP rods in slabs changes the shear punching area from around the column to the outside of the strengthened area. This confirms the hypothesis that this new area should be investigated as the real punching shear area. Two failure modes were found to take place in the new shear area under ultimate load which was based on the strengthening material used; namely, debonding of FRP rods due to epoxy resign and rupture of FRP rods

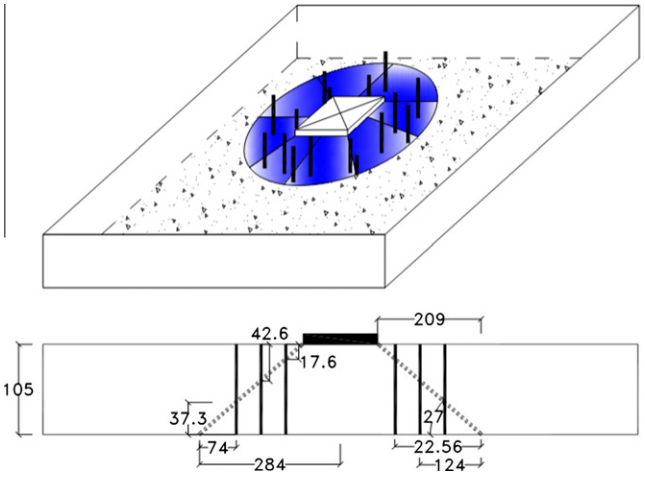

Fig. 13. Shear punch cone, strengthening line and middle plane section in slabs.

due to maximum allowed capacity of FRP rods. The failure is similar to that in strengthened beams with NSM–FRP rods studied by De Lorenzis and Nanni [12]. Therefore, their relations were generalized to the case of slabs strengthened with FRP rods without end bearings.

De Lorenzis and Nanni [12] proposed the main relations for two-dimensional cases. In the current case, however, there is a two-way slab which exhibits a three-dimensional system since there is a punching shear cone, rather than a cracked plane, that must be taken into account (Fig. 13). Based on the crack patterns obtained from experimental results, it can be concluded that the shear punching cone extends from near the column side or plate load on top to the outside area of the strengthened bottom part of the slab at a distance between d and $2d$. To adopt a common approach in all cases, the shear punch cone edge was assumed to start from the loading plate edge on the slab top to a point at a distance equal to the effective depth, d, from the strengthened bottom area of the slab (Fig. 13). This cracked cone intersects all the FRP rods as shown in Fig. 13 that depicts the section in the middle plane of the slab.

The nominal shear capacity of the slab can be calculated as in

$$V_{Punch} = V_c + V_{FRP} \tag{4}$$

where V_c is the nominal shear strength of concrete that can be obtained either from Eq. (8) in JSCE [13], or alternatively from Eqs. (13) and (14) in ACI 318-05 [14]or by using the value for the punching shear load of the corresponding control slab if some experimental test results are available. According to De Lorenzis and Nanni [12], V_{FRP} is the nominal shear strength provided by FRP rods. Two failure modes must be considered for calculating the value of V_{FRP}: the bond-controlled shear failure designated by V_{F1}, and the shear resisted by FRP rods designated as V_{F2}. The minimum value of the sum of V_{F1} and V_{F2} will be chosen as V_{FRP}.

Adopting the De Lorenzis and Nanni's [12] approach to the slab case, V_{F1} can be calculated as the sum of forces resisted by the shear bond around FRP rods intersected by the shear punch cone. This force is due to bond strength as the summation of average bond strengths around FRP rods with respect to the smallest length of the FRP rods divided by the shear punch cone edge as in Eq. (5) (see Fig. 13).

$$V_{F1} = m\pi d_{frp}\tau_b L_{tot} \tag{5}$$

where d_{frp} is FRP rod diameter; τ_b is the average bond strength; L_{tot} is the sum of effective lengths of all the rods crossed by the shear cone in one line of strengthening around the column in which, according to De Lorenzis and Nanni [12], the effective length of the FRP rod is its smallest length divided by the shear cone edge; and m is the number of strengthening lines from the center towards the edges of the slab (Fig. 13). In this case, the values for m will be 4 and 8 for 8 and 24 FRP rods, respectively. Because the slab depth or FRP rod height is less than $24d_{frp}$, according to De Lorenzis and Nanni [12], the average bond strength, τ_b, will be uniform and constant.

Based on the test results, strains in the FRP rods were less than the maximum allowed strain for FRP rods (i.e. 4000 με); so, only the loads produced in the FRP rods had to be calculated. The reason for this behavior lies in the fact that, compared to other structural elements, flat slabs are too short in terms of their depth so that FRP rod lengths do not allow for too many loads to be distributed in them via the FRP–concrete bonds; hence, few loads will be produced in FRP strengtheners. This behavior can be shown by the minimum effective length of FRP rods, $\overline{L_i}$ proposed by De Lorenzis and Nanni [12] in an equilibrium which yields a maximum allowed strain in FRP rods equal to 4000 με as calculated from

$$\overline{L_i} = \frac{d_{frp}E_{frp}}{1000\tau_b} \tag{6}$$

where E_{frp} is the Young's modulus of FRP rod. Using Eq. (6), the minimum effective length for this case study will be equal to 150 mm, indicating that the minimum FRP rod length or slab depth must be higher than 300 mm; a value which is quite uncommon in flat slabs. Hence, it is assured that none of the FRP rods will rupture. Unlike the study by De Lorenzis and Nanni [12], in the present study of FRP rod contribution to slab shear capacity, it is only needed to calculate the force produced in FRP rods (Eq. (7)), i.e. the contribution by FRP shear strength, V_{F2}.

$$V_{F2} = \sum A_{frp}f_{frp} = \sum A_{frp}E_{frp}\varepsilon_{frp} \tag{7}$$

where A_{frp} is the cross area of FRP rod and ε_{frp} is the strain in the FRP rod that will be established from the data obtained from the strain gauge installed on FRP rods.

Predicted loads for the strengthened slabs are calculated based on the presented mechanism and shown in Table 6. Here, the average bond strength (τ_b) is taken to be equal to 10 MPa as reported by the epoxy manufacturer; m is 4 for 8 FRP rods and 8 for 24 FRP rods; L_{tot} is measured at the slab section which will be the sum of the effective lengths 17.6, 42.6, and 37.3 mm (Fig. 13) in the case of FR3-24; and ε_{frp} is the FRP rod strain obtained from test results. For V_c, the corresponding values of JSCE code [13] for the un-strengthened case is used ignoring the member factor since it is only a safety factor.

The ratio of test results to the predicated loads of FRP rods (V_{Test}/V_{Punch}) yielded the values 1.6%, 8.5%, and 9.1%, respectively, for FR2-8, FR3-8, and FR3-24. This means an average error of 6.4% and a maximum error of 9.1%, which are less than 10%.

Table 6
Comparison of test and predicted FRP results.

Specimen	m	L_{tot} (mm)	V_{F1} (kN)	$\sum\varepsilon_{frp}$	V_{F2} (kN)	V_{FRP} (kN)	V_C (kN)	V_{Punch} (kN)	V_{Test} (kN)	V_{Test}/V_{Punch}
FR2-8	4	72	113.04	3600	52.96	53.0	191.1	244.1	248	1.02
FR3-8	4	72	113.04	3560	52.38	52.4	211.5	263.9	286.2	1.09
FR3-24	8	97.5	306.2	27760	408.6	306.2	211.5	517.7	412	0.80

Average and maximum errors obtained for the case of slabs are 21% and 38% less than those in the case of beams reported by De Lorenzis and Nanni [12]. The results, therefore, agree well with the experimental values of shear capacity obtained for the slabs studied and they are even better than those reported by De Lorenzis and Nanni [12] for beams. Based on the calculations, the bond failure is the prevalent mechanism in all the slabs strengthened with FRP rods as witnessed by the failure in FR2-8 and FR3-8 caused by V_{F1} but that in FR3-24 is due to V_{F2}. This means that the FRP rods in FR2-8 and FR3-8 had a lower bonding capacity than did the bond around FRPs so that V_{F2} was governed. This is while the bonding capacity around FRPs in FR3-24 was less than that of the FRP rod so that V_{F1} was governed.

5. Conclusions

In this study, the punching shear behavior of slabs strengthened by FRP rods was investigated. Epoxy resin was used for installing FRP rods. Two slabs with different reinforcement ratios and steel types were used as control. The experimental slabs consisted of one strengthened with screws and nuts, and three slabs strengthened with FRP rods. Based on the results obtained from the experiments, the following conclusions may be drawn:

1. In the slab with 8 FRP rods, an increase in shear capacity equal to 17% was obtained compared to that obtained for the control; the punching shear failure mode was observed in both slabs.
2. In the slab with 24 FRP rods, an increase in shear capacity equal to 67% was obtained compared to that obtained for the control; the flexural failure mode was observed in both slabs.
3. Increasing the number of FRP rods not only increased the shear capacity of the slab but also changed the failure mode from a punching shear to a flexural one.
4. In the slab with 8 screws and nuts, an increase in shear capacity equal to 20% was obtained compared to that obtained for the control.
5. Slabs with 8 screws and nuts and FRP rods exhibited nearly similar values of increased punching shear although the cross area of the screws was by 116% higher than that of the FRP rods. However, they exhibited different behaviors in that screws and nuts showed a flexural failure mode, but FRP rods showed a shear failure mode.
6. Comparison with pure punching shear as predicted by the equations showed 5–33% increase in the strengthened slabs, which indicated that the results were acceptable.
7. Comparison with the bond developed in the control as indicated by the equations for the slab case showed an average error of 6.4% and a maximum error of 9.1%, which are 21% and 38%, respectively, less than those for beam results. The results, therefore, show a good agreement with experimental values of shear capacity for the tested slabs and they are even better than those reported for beams.
8. The results indicate that the dominant failure mode for flat slabs strengthened with FRP rods is the deboning of FRP rods due to the small depth of slabs although this short depth increases the shear capacity of the slab up to a reasonable value and may change the slab failure mode.
9. The increased load capacity and the crack pattern of the different slabs studied showed the efficiency of the proposed strengthening method.

Acknowledgments

Isfahan University of Technology (IUT) and Nagoya University, the faculty members and the civil engineering laboratory staff and students are highly appreciated for their support and help. Dr. E. Roustazadeh from the English Department of IUT is also acknowledged for English editing services.

Appendix A

According to JSCE [13], the punching shear capacity is calculated using Eq. (8) as follows:

$$V_{pcd} = \beta_d \cdot \beta_p \cdot \beta_r \cdot f'_{pcd} \cdot u_p \cdot d/\gamma_b \tag{8}$$

where

$$f'_{pcd} = 0.20\sqrt{f'_{cd}} \quad \text{and} \quad f'_{pcd} \leqslant 1.2\ (\mathrm{N/mm^2}) \tag{9}$$

$$\beta_d = \sqrt[4]{1000/d} \leqslant 1.5 \tag{10}$$

$$\beta_p = \sqrt[3]{100\rho} \leqslant 1.5 \tag{11}$$

$$\beta_r = 1 + 1/(1 + 0.25u/d) \tag{12}$$

where f'_{cd} is the design compressive strength of concrete ($\mathrm{N/mm^2}$); u is the peripheral length of the loaded area; u_p is the peripheral length of the design cross section in the punching shear; d and ρ are average values of effective depth and reinforcement ratio in both directions of the slab, respectively, and γ_b is the member factor generally taken to be equal to 1.30.

According to ACI 318 [14], the punching shear capacity is calculated as the minimum of Eqs. (13) and (14) as follows;

$$V_c = \frac{1}{3}\sqrt{f'_c} b_0 d \tag{13}$$

$$V_c = \left(\frac{\alpha_s d}{b_0} + 2\right)\frac{\sqrt{f'_c}}{12} b_0 d \tag{14}$$

where V_c is the punching shear capacity of a 2-way slab; b_0 is the peripheral length of the design cross section in the punching shear; d is the average value of the effective depth; f'_c is the concrete compression strength; and α_s is equal to 40 for interior columns like those used in this study.

References

[1] Hassanzadeh G, Sundqvist H. Strengthening of bridge slabs on columns. Nordic Concrete Research: The Nordic Concrete Federation, publication no. 21; 1998. Paper no. 2.
[2] Polak MA. Ductility of reinforced concrete flat slab–column connections. Comput-Aid Civ Infrastruct Eng 2005;20:184–93.
[3] Martinez-Cruzado JA, Qaisrani AN, Moehle JP. Post-tensioned flat plate slab–column connections subjected to earthquake loading. In: Proceedings of 5th US national conference on earthquake engineering. Chicago, Illinois; July 1994. p. 139–48.
[4] Binici B. Punching shear strengthening of reinforced concrete slabs using fiber reinforced polymers. PhD dissertation, Department of Civil and Environmental Engineering, University of Texas at Austin, Austin, Texas; 2003. p. 279.
[5] Erki MA, Heffernan PJ. Reinforced concrete slabs externally strengthened with fibre-reinforced plastic materials. Non-metallic (FRP) reinforcement for concrete structures. In: Proceedings of second international RILEM symposium (FRPRCS-2); 1995. p. 509–16.
[6] Harajli MH, Soudki KA. Shear strengthening of interior slab–column connections using carbon fiber-reinforced polymer sheets. J Compos Constr 2003;7(2):145–53.
[7] El-Salakawy E, Soudki KA, Polak MA. Punching shear behavior of flat slabs strengthened with fiber reinforced polymer laminates. J Compos Constr 2004;8(5):384–92.
[8] Mosallam AS, Mosalam KM. Strengthening of two-way concrete slabs with FRP composite laminates. Constr Build Mater 2003;17(1):43–54.
[9] Mostafa AAEB. Development of a new FRP anchor for externally bonded CFRP sheet/laminate to beams. Master of Applied Science thesis, Carleton University, Ottawa, Ontario, Canada; 2005. 201pp.
[10] Stark A, Binici B, Bayrak O. Seismic upgrade of reinforced concrete slab–column connections using carbon fiber-reinforced polymers. ACI Struct J 2005;102(2):324–33.

[11] Moe J. Shearing strength of reinforced concrete slabs and footing under concentrated loads. Development department bulletin no. D47. Portland Cement Association; 1961; Skokie I11. p. 130.
[12] De Lorenzis L, Nanni A. Shear strengthening of RC beams with near surface mounted FRP rods. Struct J Am Concr Inst 2001;98(1):60–8.
[13] JSCE Guidelines for Concrete. Standard specification for concrete structures; 2007. p. 166.
[14] ACI Committee 318. Building code requirements for structural concrete (ACI 318-08) and commentary (318R-08). American Concrete Institute, Farmington Hills, Mich.; 2008.